Sb overlayers on (110) surfaces of III-V semiconductors: Total-energy minimization and surface electronic structure

C. Mailhiot and C. B. Duke
Xerox Webster Research Center, 800 Phillips Road, W-114, Webster, New York 14580

D. J. Chadi
Xerox Palo Alto Research Center, 3333 Coyote Hill Road, Palo Alto, California 94304

(Received 7 September 1984)

The atomic geometry, chemical bonding, and surface-state eigenvalue spectra are predicted for saturated (1×1) ordered monolayers of Sb on the (110) surfaces of GaP, GaAs, GaSb, InP, InAs, and InSb. These predictions are based on an extension of the sp^3s^* tight-binding model to encompass the calculation of total energies and hence the identification of minimum-energy surface geometries. The predicted geometries are in good correspondence with those obtained from low-energy electron diffraction for the only two cases in which the latter are known, i.e., GaAs and InP. With the use of these predicted geometries, the energy-dispersion relations of the surface states are evaluated throughout the surface Brillouin zone and compared with their clean-surface analogs. Examination of the electronic structure of these Sb-substrate systems reveals a novel type of bonding not found in either bulk III-V semiconductors or molecular III-V analogs.

I. INTRODUCTION

Considerable attention recently has been devoted to the investigation of the electronic structure and the surface chemistry of compound semiconductor interfaces via the study of adsorbate atoms on specific surfaces.[1] Since the atomic geometries of the clean (110) surfaces of III-V semiconductors are known to a fairly high degree of accuracy,[2] these surfaces constitute ideal systems to examine. Indeed, the adsorption of column-III and column-V elements on the (110) surfaces of III-V compounds has been the topic of extensive experimental[1,3–10] and theoretical[11–16] activity, the prototypical substrates being GaAs(110) (Refs. 1 and 3–8) and InP(110) (Refs. 9 and 10). In this paper we present a calculation of the atomic geometries and surface-state spectra of Sb on these and other III-V materials and compare the predictions of this calculation with the available experimental measurements.

The deposition of Sb on GaAs(110) (Refs. 1, 7 and 8) and InP(110) (Ref. 10) at room temperature produces a stable, ordered adsorbate structure at a coverage of approximately one monolayer (ML). In both systems, room-temperature adsorption of a monolayer of Sb yields an ordered overlayer structure with the same symmetry as the clean (110) surface [i.e., a $p(1\times1)$ structure]. Although several different atomic geometries have been proposed[1,4,8] for GaAs(110)-$p(1\times1)$-Sb(1 ML), dynamical analysis of measured elastic low-energy electron diffraction (ELEED) intensities[8] favors a structure in which the two Sb species in the saturated monolayer are located at sites analogous to those which would be occupied by Ga and As at an unreconstructed (110) surface. That is, the Sb species form a zigzag chain bonded to a nearly unrelaxed GaAs(110) substrate. In this geometry, the larger Sb—Sb bond length relative to that of Ga—As is accommodated by a lateral expansion of the Sb-Sb distance along the [100] direction, thereby reducing the angle between the Sb atoms within the chain from a value characteristic of tetrahedral bonding ($\Theta=109.47°$) to a value of Θ(Sb—Sb—Sb)$\sim91°$ characteristic of p^2 bonding. A schematic diagram of this structure is shown in Fig. 1 along with the definitions of various structural parameters. Among the structural parameters that characterize such an atomic geometry, the relative displacement per-

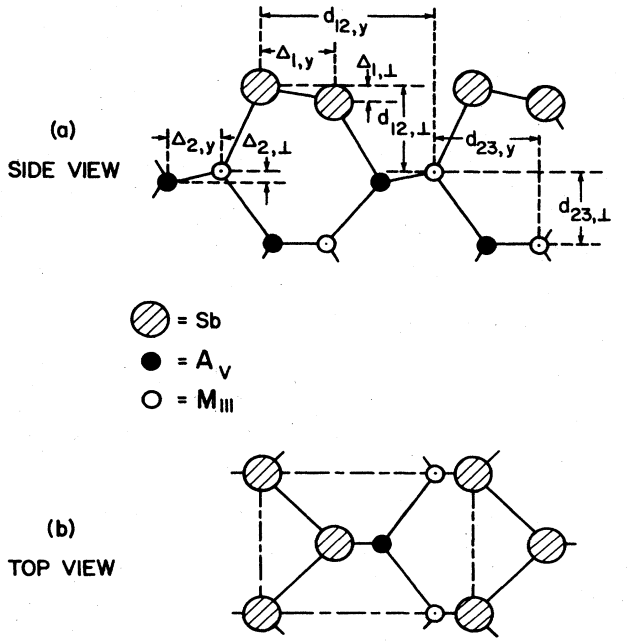

FIG. 1. Schematic diagram of the surface geometry for $M_{III}A_V(110)$-$p(1\times1)$-Sb(1 ML) and definition of the structural parameters. (a) Side view. (b) Top view.

pendicular to the (110) surface of the two Sb atoms, $\Delta_{1,\perp}$, is the one most accurately determined by ELEED (to within ± 0.05 Å). No detailed ELEED intensities analyses of InP(110)-$p(1\times1)$-Sb(1 ML) have yet been published, although some limited photoemission measurements are available.[10] Extensive angle-resolved photoemission spectroscopy (ARPES) studies are required in order to assess surface atomic geometries, however, because only the energy spectrum of surface states far away from the center of the two-dimensional Brillouin zone depends in a sensitive way on the atomic surface relaxation.[17] For example, in the case of the surface-state eigenvalue spectra associated with the clean (110) surfaces of III-V semiconductors, it was found[17] that the energy at the corner of the surface Brillouin zone of the topmost occupied surface state was quite sensitive to the position of the top-layer atoms perpendicular to the (110) surface, but fairly invariant with respect to their coordinates parallel to the surface. Suitable data are not yet available for any of the systems which we examine.

We present herein a comprehensive systematic study of the electronic, atomic, and chemical structures of ordered monolayers of Sb on the (110) surface of III-V zinc-blende structure compound semiconductors. Among the various semiconductor systems for which the chemisorption of Sb has been studied, GaAs(110) and InP(110) are the ones where both experimental data and theoretical analyses are most extensive, although still fragmentary. Consequently, we limit our study to the systems GaA_V(110)-$p(1\times1)$-Sb(1 ML) and InA_V(110)-$p(1\times1)$-Sb(1 ML), where A_V is a column-V element, namely P, As, and Sb. The major unexpected prediction of our analysis is that of a new type of hybrid chemical bond responsible for the bonding of the chemisorbed Sb chain onto the underlying substrate. This type of bonding is not present in either bulk III-V semiconductors or molecular III-V analogs, and hence seems to be a uniquely surface phenomenon resulting from the geometrical constraints which epitaxial growth of the Sb monolayer places upon the formation of chemical bonds.

The paper is organized into four parts. In Sec. II we present the theoretical formalism and the computational tools used for the determination of the atomic structures by total-energy minimization and for the calculation of the surface-state eigenvalue spectra by scattering theory. The major results relevant to the atomic geometries, surface-state eigenvalue spectra, and chemical bonding of ordered Sb overlayers are presented in Sec. III. A synopsis is given in Sec. IV.

II. THEORETICAL METHODS

In this section we describe the theoretical formalism and the computational tools which we utilize for the analysis of ordered Sb monolayers on the (110) surfaces of III-V semiconductors.

A. Tight-binding model: bulk one-electron eigenvalue spectra

In our calculations we use the first-nearest-neighbor sp^3s^* empirical tight-binding model of Vogl *et al.*,[18] because the addition of an excited s-like state s^* to the usual sp^3 minimal basis set has the effect of reducing the energy of the indirect conduction-band minimum by coupling to the antibonding p-like conduction-band states. Consequently, this model reproduces the indirect conduction band of GaP while avoiding the use of a large number of adjustable parameters. The tight-binding interactions for GaP, GaAs, GaSb, InP, InAs, and InSb are given in Table I using standard notation.[19,20] The bulk energy bands for all six substrate materials predicted by this model are, of course, identical to those given in Ref. 18, where they are compared explicitly to pseudopotential calculations and selected experimental measurements.

B. Total-energy minimization

The atomic geometries of ordered Sb monolayers on the (110) surfaces of Ga—A_V and In—A_V were determined via total-energy minimization procedures within the empirical sp^3s^* tight-binding formalism outlined above. The theoretical framework has been described elsewhere and applied to the determination of the atomic structure of various clean semiconductor surfaces.[21] Within this model the variation of the total energy associated with atomic displacements is given by

$$\Delta E_{\text{total}} = \sum_{\substack{n\mathbf{k} \\ \text{occupied}}} \Delta E_n(\mathbf{k}) + \sum_{i\neq j}\sum_{m} U_m \epsilon_{ij}^m , \tag{1}$$

in which the first term on the right-hand side of Eq. (1) represents the contribution due to the band-structure energy, while the second term is an empirical correction for the double counting of electron-electron interactions in the band-structure energy and includes the ion-ion interaction energy.

The $E_n(\mathbf{k})$ comprise the eigenvalue spectrum associated with one-electron states $|n\mathbf{k}\rangle$ calculated using the model described in Sec. II A. The quantity ϵ_{ij} is the fractional change in bond length between the atoms labeled i and j with respect to the bulk value. In the summation of the second contribution, we retain only up to quadratic terms ($m=1,2$) in the fractional bond-length changes ϵ_{ij}. The empirical elastic constants U_m are determined, for the III-V substrates, by adjusting them to fit bulk elastic moduli and phonon frequencies and by requiring that ΔE_{total} has no contribution from linear terms in the atomic displacements. The parameters U_1 and U_2 for all of the six substrate materials also are given in Table I. The determination of these parameters and the application of the sp^3s^* model to predict atomic geometries constitute extensions of the models developed earlier by Vogl *et al.*[18] and by Chadi,[21] respectively.

The variation in the one-electron eigenvalue spectrum $E_n(\mathbf{k})$ resulting from atomic displacements is calculated by assuming a d^{-2} dependence of the transfer tight-binding interactions on first-nearest-neighbor distance, d.[18,20,22] This approximation has proven to be useful for predicting changes in band-structure energy associated with atomic displacements in agreement with more complete self-consistent pseudopotential calculations.[23]

The total-energy-minimization calculations described above are performed using a finite slab, periodic in two di-

TABLE I. Empirical tight-binding interactions as obtained from Ref. 18 for the sp^3s^* model. The index 1 (2) refers to the anion (cation). The notation is that used by Chadi (Ref. 19) rather than by Vogl *et al.* (Ref. 18). The empirical parameters U_1 and U_2 obtained by fitting bulk elastic moduli and phonon frequencies using the sp^3s^* tight-binding model, also are indicated. Units are eV.

Tight-binding interactions	GaP	GaAs	GaSb	InP	InAs	InSb
$E_s[1]$	−8.112	−8.343	−7.321	−8.527	−9.538	−8.016
$E_s[2]$	−2.198	−2.657	−3.899	−1.483	−2.722	−3.464
$E_{s^*}[1]$	8.515	8.591	6.635	8.264	7.410	6.454
$E_{s^*}[2]$	7.185	6.739	5.985	7.067	6.740	5.936
$E_p[1]$	1.125	1.041	0.855	0.873	0.910	0.674
$E_p[2]$	4.115	3.669	2.915	4.047	3.720	2.916
$V_{ss\sigma}[1,2]$	−1.868	−1.613	−1.539	−1.340	−1.401	−1.380
$V_{sp\sigma}[1,2]$	1.852	1.940	2.148	0.964	1.314	1.640
$V_{sp\sigma}[2,1]$	2.736	2.504	2.021	2.417	2.355	1.987
$V_{s^*p\sigma}[1,2]$	2.015	2.097	2.161	1.499	1.461	1.544
$V_{s^*p\sigma}[2,1]$	2.206	2.082	1.826	1.941	1.693	1.474
$V_{pp\sigma}[1,2]$	3.106	3.028	2.459	2.586	2.695	2.289
$V_{pp\pi}[1,2]$	−0.746	−0.781	−0.637	−0.588	−0.657	−0.619
U_1	−18.55	−17.79	−15.84	−13.89	−14.27	−13.18
U_2	59.08	56.50	52.64	50.98	48.87	47.52

mensions, to simulate the semi-infinite solid. The slab method is also commonly used within the empirical tight-binding framework for the calculation of surface-state eigenvalue spectra.[24] Diagonalization of the tight-binding slab Hamiltonian yields the one-electron energy eigenvalue spectrum $E_n(\mathbf{k})$, which appears in Eq. (1). Surface states can be identified by studying the localization of the resulting one-electron states $|n\mathbf{k}\rangle$.

In the present work, however, we determine only the atomic geometries by use of the slab calculations described above. These geometries are used as inputs for the evaluation of surface-state eigenvalue spectra as described in the following section. Although localized surface bound states are easily identifiable and accurately described within the slab method, surface resonances are not. In order to identify surface resonances and to incorporate explicitly the semi-infinite nature of the physical system, we adopt the scattering theoretical method[22] (STM) for the calculation of surface bound states and resonances. The *same* tight-binding sp^3s^* model (given in Table I) is utilized in our calculations of *both* the atomic geometries *and* the surface-state eigenvalue spectra.

C. Surface-state eigenvalue spectra

Our calculations of the surface-state eigenvalue spectra associated with ordered Sb monolayers on the (110) surface of Ga—A_V and In—A_V are performed using the geometries determined by the total-energy minimization procedure outlined in Sec. II B. These spectra are evaluated via an analytic Green's function methodology[25] which embodies the STM.[22,26] We next briefly outline the formalism. The interested reader should consult Sec. II A of Ref. 26 for a more detailed description.

The ideal crystal bulk Green's function $G^0(\mathbf{x}\mathbf{x}';\mathbf{k}_{||},E)$ at a given parallel wave vector $\mathbf{k}_{||}$, and energy E is written, in the analytic representation,[25] as

$$G^0(\mathbf{x}\mathbf{x}';\mathbf{k}_{||},E)=-2\pi i\left[\sum_\lambda \frac{|\,\mathbf{x};\mathbf{k}_{||}k_\lambda^+\rangle\langle\mathbf{x}';\mathbf{k}_{||}k_\lambda^{+*}\,|}{v_3(\mathbf{k}_{||}k_\lambda^+)}\Theta(x_3-x_3')-\sum_\lambda \frac{|\,\mathbf{x};\mathbf{k}_{||}k_\lambda^-\rangle\langle\mathbf{x}';\mathbf{k}_{||}k_\lambda^{-*}\,|}{v_3(\mathbf{k}_{||}k_\lambda^-)}\Theta(x_3'-x_3)\right], \tag{2}$$

where $|\,\mathbf{x};\mathbf{k}_{||}k_\lambda\rangle$ is a bulk Bloch solution to Schrödinger's equation associated with a (real or complex) wave vector $\mathbf{k}_\lambda=\mathbf{k}_{||}+\hat{\mathbf{x}}_3k_\lambda$ with $\mathbf{k}_{||}$ in the plane of the surface and $\hat{\mathbf{x}}_3k_\lambda$ normal to the plane of the surface. The component of the group velocity in the direction normal to the surface, $v_3(\mathbf{k}_{||}k_\lambda)$, is defined as[25]

$$v_3(\mathbf{k}_{||}k_\lambda)\equiv\left[\frac{\partial E(\mathbf{k}_{||},k_3)}{\partial k_3}\right]_{k_3=k_\lambda}. \tag{3}$$

The solutions $\{k_\lambda\}$ are divided into two groups:[27]

$$k_\lambda\pm \text{ complex: } \mathrm{Im}[k_\lambda^\pm]\gtrless 0\,, \tag{4a}$$

$$k_\lambda^\pm \text{ real: } v_3(\mathbf{k}_{||}k_\lambda^\pm)\gtrless 0\,. \tag{4b}$$

The unit step function $\Theta(x_3)$ is defined such that $\Theta(0)\equiv\frac{1}{2}$.

In order to calculate the Green's function $G^0(\mathbf{x}\mathbf{x}';\mathbf{k}_{||},E)$ we expand the bulk Bloch states $|\,\mathbf{x};\mathbf{k}_{||}k_\lambda\rangle$ in terms of planar orbitals, $|\,\alpha\nu;\mathbf{k}_{||},\sigma\rangle$, i.e.,

$$|\,\alpha\nu;\mathbf{k}_{||},\sigma\rangle\equiv\sum_{\mathbf{R}_{||}}\exp(i\mathbf{k}_{||}\cdot\mathbf{R}_{||})\,|\,\alpha\nu;\mathbf{R}_{||}\sigma\rangle\,, \tag{5}$$

in which α labels the orbital symmetry ($\alpha=s,p_x,p_y,p_z,s^*$), ν labels the atomic plane ($\nu=$ anion, cation), and σ labels the layer. The vector $\mathbf{R}_{||}$ is the two-dimensional lattice translation vector and $|\alpha\nu;\mathbf{R}_{||}\sigma\rangle$ designates a local orbital. From these planar orbitals, we construct Bloch sums associated with wave vector $\mathbf{k}_\lambda=\mathbf{k}_{||}+\hat{\mathbf{x}}_3 k_\lambda$ via

$$|\alpha\nu,\mathbf{k}_{||}k_\lambda\rangle\equiv\frac{1}{\sqrt{N}}\sum_\sigma \exp(ik_\lambda\sigma a)\,|\alpha\nu;\mathbf{k}_{||},\sigma\rangle\ , \tag{6}$$

in which a is the interlayer spacing, and N is a normalization constant. Finally, the bulk Bloch solutions $|\mathbf{x};\mathbf{k}_{||}k_\lambda\rangle$ are written as a linear combination of Bloch sums:

$$\begin{aligned}|\mathbf{x};\mathbf{k}_{||}k_\lambda\rangle&=\sum_{\alpha\nu}C(\alpha\nu;\mathbf{k}_{||}k_\lambda)\,|\alpha\nu;\mathbf{k}_{||}k_\lambda\rangle\\&=\sum_{\alpha\nu}C(\alpha\nu;\mathbf{k}_{||}k_\lambda)\\&\quad\times\left[\frac{1}{\sqrt{N}}\sum_\sigma\exp(ik_\lambda\sigma a)\,|\alpha\nu;\mathbf{k}_{||},\sigma\rangle\right]\ ,\end{aligned} \tag{7}$$

in terms of the set of planar orbitals $|\alpha\nu;\mathbf{k}_{||},\sigma\rangle$. The expansion coefficients $C(\alpha\nu;\mathbf{k}_{||}k_\lambda)$ are evaluated by using a transfer-matrix methodology[27,28] that produces the bulk solutions to Schrödinger equation for complex $\mathbf{k}$ via the solution of an eigenvalue problem. The analytic Green's function can then be written in the planar orbital representation $\{|\alpha\nu;\mathbf{k}_{||},\sigma\rangle\}$ as[27]

$$\begin{aligned}G^0(\alpha\nu;\alpha'\nu';\sigma-\sigma';\mathbf{k}_{||},E)=-2\pi i\Bigg[&\sum_\lambda\frac{C(\alpha\nu;\mathbf{k}_{||}k_\lambda^+)C^*(\alpha'\nu';\mathbf{k}_{||}k_\lambda^{+*})}{v_3(\mathbf{k}_{||}k_\lambda^+)}\exp[ik_\lambda^+(\sigma-\sigma')a]\Theta(\sigma-\sigma')\\&-\sum_\lambda\frac{C(\alpha\nu;\mathbf{k}_{||}k_\lambda^-)C^*(\alpha'\nu';\mathbf{k}_{||}k_\lambda^{-*})}{v_3(\mathbf{k}_{||}k_\lambda^-)}\exp[ik_\lambda^-(\sigma-\sigma')a]\Theta(\sigma'-\sigma)\Bigg]\end{aligned} \tag{8}$$

where $\sigma(\sigma')$ labels the layer, $\nu(\nu')$ labels the atomic plane within the layer, and $\alpha(\alpha')$ labels the orbital symmetry type.

The Hamiltonian for the overlayer system, H, is related to the Hamiltonian of the perfect crystal, H_0, by

$$H=H_0+U\ , \tag{9}$$

where U is the perturbation matrix that formally describes the creation of the surface, the formation of the monolayer system, and the surface atomic relaxation.[26] The Green's function of the perturbed (overlayer) system, $G(E)$, is related to the bulk Green's function $G^0(E)$ by Dyson's equation[26]

$$G(E)=G^0(E)+G^0(E)UG(E)=[1-G^0(E)U]^{-1}G^0(E)\ . \tag{10}$$

The perturbation matrix used within the scattering theoretical method is obtained in three steps: (i) cleavage of the crystal along a (110) plane, (ii) replacement of the topmost layer by a monolayer of Sb atoms, and (iii) geometrical relaxation of the surface atom according to the total-energy minimization results. The formal application of the STM, applied here to overlayer systems, is described in Refs. 26 and 29.

Once the Green's function for the perturbed system (i.e., overlayer) and the perturbation matrix are known, the energies E of a bound surface state are determined by the solutions to[26]

$$\det[1-G^0(E)U]=0\ . \tag{11a}$$

Similarly, surface resonances can be identified by the total change in the density of states[26]

$$\Delta N(E)=\frac{1}{\pi}\,\mathrm{Tr}\{\,\mathrm{Im}[G(E)-G^0(E)]\}\ . \tag{11b}$$

We adopt, however, the effective Hamiltonian method developed by Beres *et al.*,[30] in order to locate surface bound states and surface resonances. This method has already been applied by these authors to the (110) surfaces of III-V semiconductors.[30,31] In this method, an effective Hamiltonian $H_{\mathrm{eff}}(E)$ is defined by

$$E-H_{\mathrm{eff}}(E)\equiv G^0(E)^{-1}-U\ , \tag{12}$$

where $G^0(E)$ is the bulk Green's function in the subspace of the perturbation. Let the eigenvalues of $H_{\mathrm{eff}}(E)$ be $\lambda_i(E)$. In the energy-band gap, the eigenvalues $\lambda_i(E)$ are real and the condition for a surface bound state of energy E is

$$\lambda_i(E)=E\ . \tag{13a}$$

In the bulk energy bands, the eigenvalues $\lambda_i(E)$ are complex and the condition for a surface resonance at the energy E is[30]

$$\mathrm{Re}[\lambda_i(E)]=E\ . \tag{13b}$$

Thus, the analytic Green's function and the effective Hamiltonian provide a convenient framework for the computation of surface bound states and surface resonances that is technically superior to conventional slab methods.

D. Extension to Sb overlayers

The sp^3s^* tight-binding model has been applied to interpret successfully data on bulk point defects,[32] bulk,[33] and surface[34] core excitons, and semiconductor surface states.[35] More recently it has been utilized to predict the structural phase transitions of the Si(100) surface as a function of temperature.[36] Of most importance from our perspective, the model has been shown to provide atomic surface structures for the clean (110) surfaces of GaP, GaAs, GaSb, InP, InAs, and InSb in quantitative agree-

ment with dynamical analyses of measured ELEED intensities.[37] In every empirical analysis, however, the question of determining the parameters is a delicate one, and the present tight-binding model is no exception.[38] Within the present calculation, the tight-binding transfer matrix elements between the two Sb atoms of the overlayer and between the Sb atom and the column-V element of the substrate are unknown. To obtain the first-nearest-neighbor transfer interactions, we scale the interactions of GaSb (for Sb on GaP, GaAs, and GaSb) and those of InSb (for Sb on InP, InAs, and InSb) by a d^{-2} scaling law. Therefore we obtain the transfer matrix elements

$$V(\alpha\alpha';\mathrm{Sb}-A_{\mathrm{V}})=V(\alpha\alpha';\mathrm{Sb}-M_{\mathrm{III}})\left[\frac{d(\mathrm{Sb}-M_{\mathrm{III}})}{d(\mathrm{Sb}-A_{\mathrm{V}})}\right]^{2}, \tag{14}$$

where α,α' label the orbital symmetry $(s;p_x,p_y,p_z;s^*)$, $M_{\mathrm{III}}=$ Ga (In) for Sb on GaP, GaAs, GaSb (InP, InAs, InSb), and $A_{\mathrm{V}}=$P, As, Sb. We therefore obtain two set of tight-binding transfer interactions, corresponding to the Ga—A_{V} and In—A_{V} substrates, respectively. The Sb—M_{III} bond lengths are determined by the sum of the covalent radii.[39] The Sb—A_{V} bond lengths were determined from bulk Sb for Sb—Sb bonds, $Sb_{1-x}As_x$ alloys for Sb—As bonds, and from the ELEED structure analysis of InP(110)-$p(1\times1)$-Sb(1 ML) for Sb—P bonds. The tight-binding transfer matrix elements obtained by this prescription are given in Table II for GaA_{V}(110)-$p(1\times1)$-Sb(1 ML) and in Table III for InA_{V}(110)-$p(1\times1)$-Sb(1 ML). The on-site energies (E_s, E_s^*, E_p) for Sb were taken to be those of GaSb (InSb) for Sb on GaP, GaAs, and GaSb (InP, InAs, and InSb). These energies are given in Table I. We have tested this scheme by scaling the transfer matrix elements in different fashions. Numerical tests reveal that the resulting surface atomic geometries are in qualitative correspondence to the ones obtained using the simple d^{-2} scaling law described above. Therefore the results given in Tables II and III seem adequate for our purposes.

TABLE II. Empirical tight-binding transfer interactions between Sb and the substrate column-V element for GaA_{V}(110)-$p(1\times1)$-Sb(1 ML). d_0 designates the Sb—A_{V} bond length. The index 1(3) refers to the column-V element (Sb). The notation is that of Chadi (Ref. 19). The empirical parameters U_1 and U_2, obtained from a Sb$A_{\mathrm{V}}H_6$ cluster calculation, are also indicated. Units for the interactions are eV and for the bond lengths are Å. The Sb—Ga bond length is taken to be 2.65 Å.

Tight-binding interactions	Sb—P	Sb—As	Sb—Sb
$V_{ss\sigma}[1,3]$	−2.428	−1.649	−1.312
$V_{sp\sigma}[1,3]$	3.188	2.166	1.777
$V_{sp\sigma}[3,1]$	3.388	2.302	1.777
$V_{s^*p\sigma}[1,3]$	3.409	2.316	1.700
$V_{s^*p\sigma}[3,1]$	2.880	1.957	1.700
$V_{pp\sigma}[1,3]$	3.879	2.635	2.096
$V_{pp\pi}[1,3]$	−1.005	−0.683	−0.543
U_1	−19.36	−17.70	−14.92
U_2	59.08	56.50	52.64
d_0	2.11	2.56	2.87

TABLE III. Empirical tight-binding transfer interactions between Sb and the substrate column-V element for InA_{V}(110)-$p(1\times1)$-Sb(1 ML). d_0 designates the Sb—A_{V} bond length. The index 1(3) refers to the column-V element (Sb). The notation is that of Chadi (Ref. 19). The empirical parameters U_1 and U_2, obtained from a Sb$A_{\mathrm{V}}H_6$ cluster calculation, are also indicated. Units for the interactions are eV and for the bond lengths are Å. The Sb—In bond length is taken to be 2.81 Å.

Tight-binding interactions	Sb—P	Sb—As	Sb—Sb
$V_{ss\sigma}[1,3]$	−2.448	−1.663	−1.323
$V_{sp\sigma}[1,3]$	2.909	1.976	1.738
$V_{sp\sigma}[3,1]$	3.524	2.394	1.738
$V_{s^*p\sigma}[1,3]$	2.738	1.860	1.447
$V_{s^*p\sigma}[3,1]$	2.614	1.776	1.447
$V_{pp\sigma}[1,3]$	4.060	2.758	2.194
$V_{pp\pi}[1,3]$	−1.098	−0.746	−0.593
U_1	−18.55	−16.91	−14.21
U_2	50.98	48.87	47.52
d_0	2.11	2.56	2.87

In order to determine the empirical elastic parameters U_m for the Sb—A_{V} bonds, we performed a Sb$A_{\mathrm{V}}H_6$ cluster calculation assuming tetrahedral bonding. The elastic parameter U_1 is then determined by varying the length of the Sb—A_{V} bond and requiring that the resulting changes in the total energy do not contain any linear term in the fractional bond-length changes, ϵ. To perform this calculation, the energy eigenvalue spectrum of the cluster is determined by using the same set of on-site parameters for the column-V element corresponding to a given substrate, i.e., Ga—A_{V} and In—A_{V} parameters for Ga and In compounds, respectively. The empirical tight-binding parameters corresponding to the Sb—A_{V} interactions are given according to the scaling law Eq. (14). The value of U_2 was taken to be equal to that of the substrate.

Due to the somewhat arbitrary nature of the scaling relation Eq. (14), the resulting surface structures cannot be regarded as quantitative predictions since their details depend on the value of the input parameters. Numerical tests reveal that an increase of 15% in the value of the tight-binding parameters associated with the Sb—A_{V} interactions translates in an increase of the structural parameter $\Delta_{1,\perp}$ by as much as about 70% to 80% for the Ga—A_{V} substrates and about 40% to 45% for the In—A_{V} substrates. Therefore, in view of the fact that Eq. (14) is dependent on the input value of the Sb—A_{V} bond length, the quantitative details of the resulting structures are parameter dependent. Although these observations suggest caution in evaluating the quantitative validity of our surface structure predictions, they do not influence in any important way our interpretation of the nature of the chemical bonding. Furthermore, the surface-state eigenvalue spectra shown below are nearly invariant with respect to variations in the quantitative structural details of the sort considered here for a given type of class of structure.

E. Computational details

The minimization of the total energy is performed on a slab of 14 atomic layers periodic in two dimensions. Relaxation within the outermost three layers is included in the model. The calculational procedure follows that outlined by Chadi.[21] The major innovation relative to earlier calculations[21] is the use of an automatic Hellmann-Feynman gradient program[40] to locate the minimum-energy structure automatically rather than to search the surface-geometry parameter space manually.

The starting structure is obtained from the ELEED intensity analysis of Ref. 8, i.e., Sb atoms are substituted for the top-layer anion and cation on an unreconstructed (110) surface. This structure is referred to as model 2 in Ref. 1, and is shown in Fig. 1. Although we also searched for minimum-energy structures corresponding to different attachments of the Sb chains on the substrate (specifically model 1 in Ref. 1), we find that the minimum-energy structures always are of the type suggested by the ELEED analysis of Ref. 8. This result is invariant under the small changes in model input parameters discussed in Sec. II D.

Given the minimum-energy surface atomic geometries, the surface-state eigenvalue spectra of both the clean and Sb covered (110) surfaces are evaluated as described in Sec. II C. Since second-layer relaxations are generally small, the perturbation matrix is taken to affect only the two top layers in the calculation of the surface-state eigenvalues spectra. The surface-state energy dispersions are obtained directly by locating the surface bound states and surface resonances at various points of the two-dimensional Brillouin zone via the effective Hamiltonian method described at the end of Sec. II C. Verification of the energies of the surface bound states is done by inspection of the orbital-resolved local density of state obtained directly from the Green's-function matrix. Detailed understanding of the bonding and antibonding nature of the surface states can only be achieved, however, by analysis of the energy eigenvectors associated with the slab Hamiltonian. With the combined use of the analytic Green's-function method and the slab Hamiltonian, we are able both to locate accurately the surface-state energies and to obtain direct access to the orbital character of the energy eigenvectors.

III. RESULTS

In this section we present our predictions of the atomic and electronic structures of ordered Sb monolayers on the (110) surface of III-V semiconductor compounds. We proceed in four steps. First, in Sec. III A we present the atomic geometries as determined via our total-energy minimization scheme within the tight-binding model outlined in Secs. II A and II B. Second, in Sec. III B we examine the surface-state eigenvalue spectra obtained for the minimum-energy geometries. The nature of the chemical bonding responsible for the bonding of the Sb chain to the underlying substrate is interpreted in the light of the results for the atomic structure and the associated surface-state eigenvalue spectra. Comparisons with the surface-state eigenvalue spectra associated with the clean (110) substrates are presented in Sec. III C. Finally, we correlate the predicted atomic structures of the Sb overlayers with the measures of the electronic inequivalence of the substrate anion and cation, as well as with the minimum-energy surface bond lengths.

A. Atomic geometries of Sb overlayers

The structural parameters characterizing the atomic geometries of ordered Sb overlayers on the (110) surface of III-V compounds are defined in Fig. 1 and specified in Table IV. The experimental results obtained by ELEED intensity analyses also are given in Table IV for the two cases in which they are known, i.e., GaAs(110)-$p(1\times1)$-Sb(1 ML) (Ref. 8) and InP(110)-$p(1\times1)$-Sb(1 ML) (Ref. 41).

The relative displacement of the two Sb atoms perpendicular to the (110) surface, $\Delta_{1,\perp}$, is determined to within ±0.05 Å by dynamical analyses of ELEED intensity data. Table IV reveals that the values of $\Delta_{1,\perp}$ predicted by our calculation are in quantitative correspondence with those obtained via ELEED data analyses for both

TABLE IV. Structural parameters predicted for the atomic geometries of $M_{III}A_V(110)$-$p(1\times1)$-Sb(1 ML) systems defined in Fig. 1. The values inclosed in parentheses were determined via ELEED for GaAs(110)-$p(1\times1)$-Sb(1 ML) (Ref. 8) and for InP(110)-$p(1\times1)$-Sb(1 ML) (Ref. 41). Units are Å and a_0 is the bulk lattice constant of the substrate.

	GaP	GaAs	GaSb	InP	InAs	InSb
a_0	5.451	5.654	6.118	5.869	6.036	6.478
$\Delta_{1,\perp}$	0.34	0.09 (0.10±0.05)	0.07	0.57 (0.70±0.1)	0.22	0.13
$\Delta_{1,y}$	1.89	1.87 (1.96±0.3)	1.80	2.02 (1.98±0.3)	1.76	1.68
$d_{12,\perp}$	2.12	2.29 (2.39±0.1)	2.25	2.23 (2.43±0.1)	2.23	2.21
$d_{12,y}$	3.91	4.39 (4.62±0.3)	4.73	4.00 (4.46±0.3)	4.34	4.74
$\Delta_{2,\perp}$	0.00	0.08 (0.10±0.05)	0.18	0.09 (0.00±0.1)	0.20	0.20
$\Delta_{2,y}$	1.36	1.42 (1.41±0.3)	1.57	1.47 (1.47±0.3)	1.54	1.68

GaAs(110)-$p(1\times1)$-Sb(1 ML) and InP(110)-$p(1\times1)$-Sb(1 ML). The values of the top-layer shear vector Δ_1 for the Sb overlayers on GaP, GaSb, InAs, and InSb remain predictions to be tested by subsequent structure analyses.

The remaining structural parameters are less accurately determined by the ELEED structure analyses. Moreover, the predictions of our tight-binding model are sensitive to the (imprecisely known) input values of the Sb-cation and Sb-anion bond lengths. The former are probably close to their values in GaSb and InSb. The latter, however, are less well known, especially for the Sb—P bond, so that the model predictions are uncertain to within several tenths of an angstrom. Given a (conservative) ±0.2 Å estimated uncertainty in the model predictions, the correspondence specified in Table IV between the predicted and measured structures is quantitative, i.e., within the combined theoretical-experimental uncertainties. The situation for GaAs is better than that for InP, in that the magnitude of the differences between the predicted and measured structural parameter lie within uncertainties inherent in the ELEED analysis alone. Also, the Sb—As bond lengths may be estimated independently from $Sb_{1-x}As_x$ alloys, whereas the Sb—P bond length must be extracted from the ELEED intensity analysis, itself.

We next examine the sensitivity of the total-energy minimization procedure to the magnitude of the structural parameters characteristic of the Sb overlayer. We study the changes in total energy resulting from various displacements of the top-layer Sb atoms with respect to their minimum-energy configuration, limiting our attention to the structural parameters $\Delta_{1,\perp}$, $d_{12,\perp}$, and $\Delta_{1,y}$. The structural parameters $\Delta_{1,\perp}$ and $d_{12,\perp}$ are most accurately determined by ELEED, whereas $\Delta_{1,y}$ is most precisely determined by ion channeling. For each substrate compound, the changes in total energy, ΔE_{total}, were calculated as a function of the variation of the associated structural parameter from its minimum-energy value given in Table IV. We obtain a universal behavior of

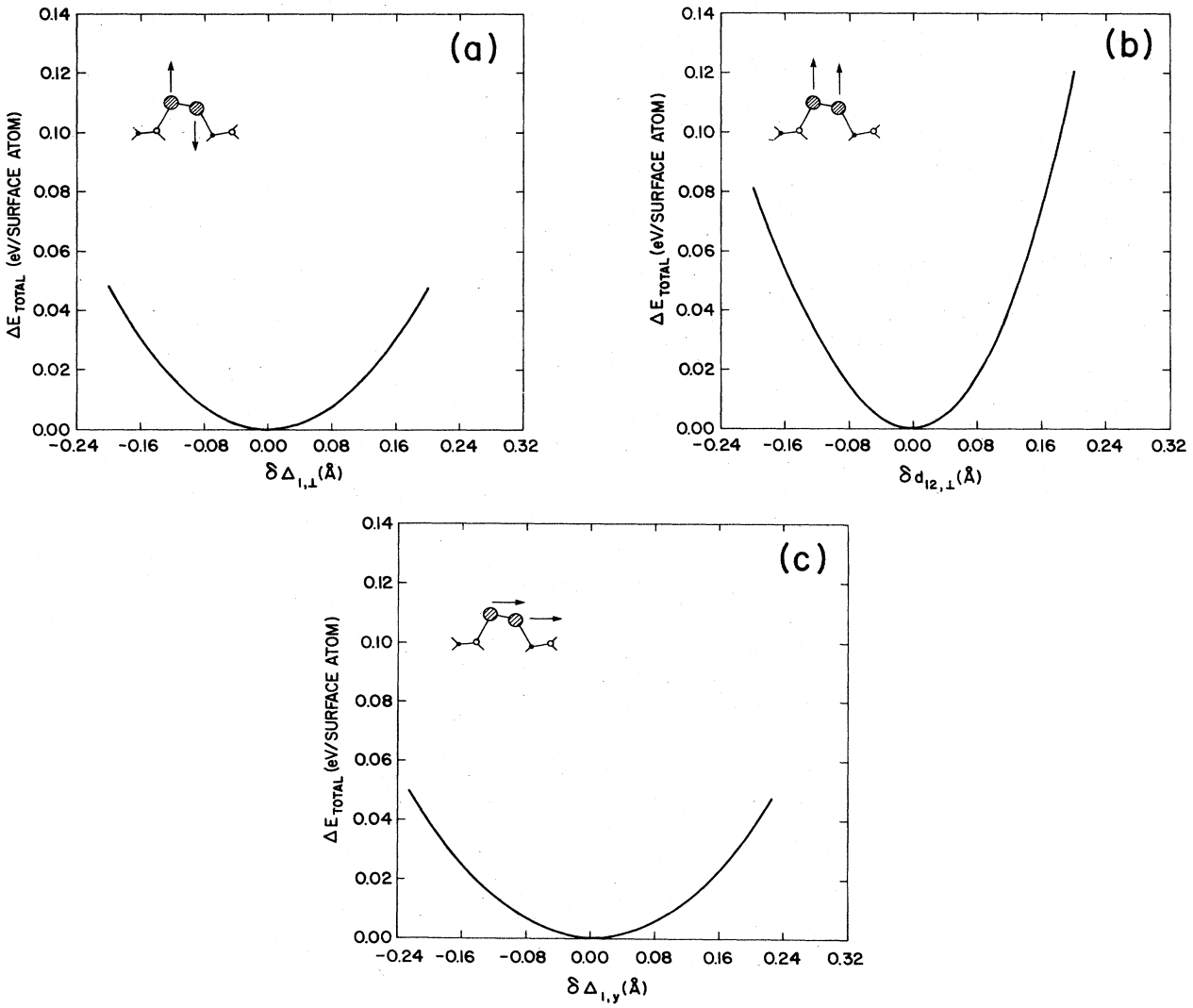

FIG. 2. Variation in total energy ΔE_{total} as a function of changes in the structural parameters with respect to their minimum-energy value as given in Table IV for GaAs(110)-$p(1\times1)$-Sb(1 ML). (a) $\Delta_{1,\perp}$. (b) $d_{12,\perp}$. (c) $\Delta_{1,y}$. The origin on the x axis represents the minimum-energy configuration. Also shown is a schematic representation of the atomic motions involved in each case.

ΔE_{total}, as a function of atomic displacements about their equilibrium position, that scales as the lattice constant of the substrate. Consequently, we display only the results for GaAs(110)-$p(1\times1)$-Sb(1 ML).

In Fig. 2 the changes in total energy are plotted as a function of the variations in the structural parameters $\Delta_{1,\perp}$, $d_{12,\perp}$, and $\Delta_{1,y}$ about their minimum-energy values for GaAs(110)-$p(1\times1)$-Sb(1 ML). As noted by Chadi,[21] variation in E_{total} of the order of 0.01 eV/surface atom is the limit of the intrinsic accuracy of the present tight-binding model. From Fig. 2 we see that variations of the atomic coordinates of the top-layer Sb atoms with respect to their minimum-energy configurations result in quadratic changes in the total energy. This behavior is built into our model by adjusting the parameters U_1 and U_2 such that ΔU cancels the linear term in the variation of the band-structure energy. Figure 2 demonstrates that the predicted geometries correspond to local minimum-energy configurations. The total energy of the system is more sensitive to variations in $d_{12,\perp}$ than it is to variations of $\Delta_{1,\perp}$ and $\Delta_{1,y}$, because variations in $d_{12,\perp}$ result in primarily bond-stretching motions, whereas variations in $\Delta_{1,\perp}$ and $\Delta_{1,y}$ result predominately in bond-bending motions. We see from Fig. 2 that the uncertainty in the model predictions (for fixed input bond lengths) is approximately ±0.1 Å: an uncertainty which must be added to that caused by imprecise knowledge of the surface bond lengths.

B. Surface-state eigenvalue spectra

We have calculated the surface-state eigenvalue spectra associated with ordered Sb monolayers on the (110) surfaces GaP, GaAs, GaSb, InP, InAs, and InSb. An understanding of the chemical bonding of ordered Sb monolayers to the substrate cannot be achieved, however, from these results alone. Rather we must begin with a study of the electronic structure of single p^2-bonded isolated chain of Sb atoms. In Fig. 3 we show the energy eigenvalue spectrum of a single Sb chain as well as the orbital character associated with different energy eigenstates, at $\mathbf{k}_{||}=0$. The energy eigenvalue spectrum of the isolated p^2-bonded Sb chain reveals three types of electronic states.

First, Fig. 3(c) reveals the existence of *nonbonding states.* These include the totally symmetric (s^+) and antisymmetric (s^-) s-like occupied lone-pair states. Our model also predicts totally symmetric (s^{*+}) and antisymmetric (s^{*-}) unoccupied s^*-like lone pairs emanating from the (unoccupied) s^* atomic orbitals. These s-like (s^*-like) states lie at low (high) energy. Since both the $s^+(s^{*+})$ and s^- (s^{*-}) states are occupied (unoccupied) they do not contribute to the bonding of the Sb atoms in the chain. Their energy and dispersion are perturbed very little by the substrate.

Second, Fig. 3(b) reveals the existence of *bonding and antibonding p^2 states in the plane of the chain.* These include occupied bonding (p_x^- and p_y^-) and unoccupied antibonding (p_x^+ and p_y^+) states that either generate a nodal plane between the Sb atoms (antibonding p_x^+ and p_y^+) or not (bonding p_x^- and p_y^-). As $\mathbf{k}_{||}$ is varied from $\bar{\Gamma}$ to $\bar{X}$, i.e., along the chain direction, the occupied bonding states

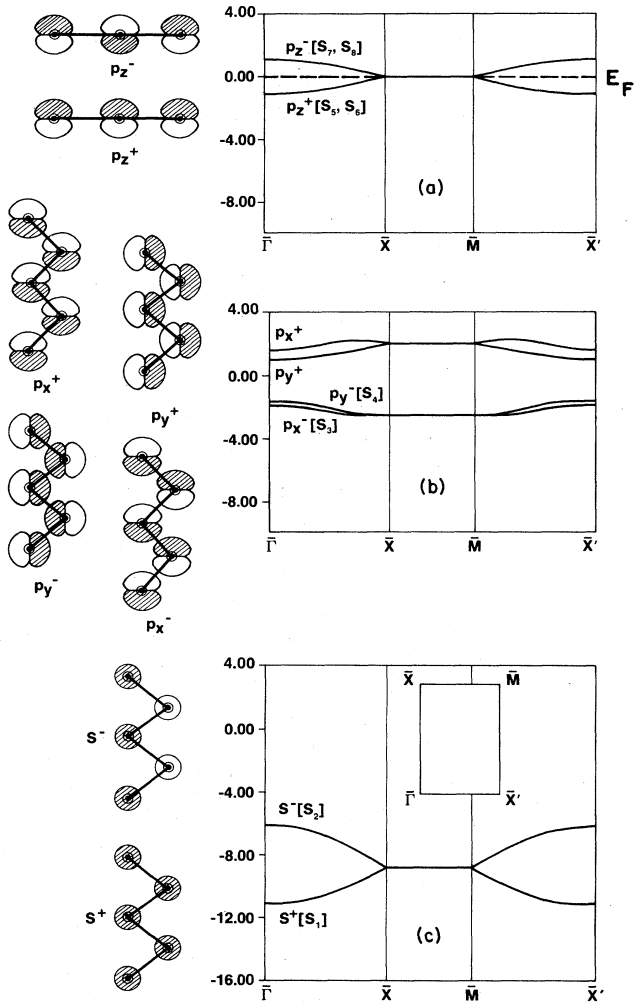

FIG. 3. Energy dispersion relation for a single isolated Sb chain mapped onto the zinc-blende (110) surface Brillouin zone. The orbital character of the energy eigenstates at $\mathbf{k}_{||}=0$ is indicated schematically. Hatched and open areas indicate positive and negative contours, respectively. (a) Energy dispersion relation for bonding (p_z^+) and antibonding (p_z^-) π-electron states. These states are only half occupied for the (metallic) isolated p^2-bonded Sb chain. The dashed line indicates the position of the Fermi level E_F. (b) Energy dispersion relation for bonding (p_x^- and p_y^-) and antibonding (p_x^+ and p_y^+) states in the plane of the chain. (c) Energy dispersion relation for symmetric (s^+) and antisymmetric (s^-) nonbonding s-like lone pairs. The inset shows the (110) surface Brillouin zone.

(p_x^- and p_y^-) mix together in such a way as to preserve a bonding character with high electronic density between the Sb atoms. Similarly, for $\mathbf{k}_{||}$ varying from $\bar{\Gamma}$ to $\bar{X}$, the unoccupied antibonding states (p_x^+ and p_y^+) mix together while retaining an antibonding character with low electronic density between the Sb atoms. The bonding states are primarily responsible for the p^2 bonding of the Sb atoms in the plane of the chain. Their participation to the bonding of the chain to the substrate is limited and, as for the s-like lone pairs, they are only slightly affected by the substrate.

Third, Fig. 3(a) reveals the existence of *bonding and antibonding π states normal to the chain.* These include bonding (p_z^+) and antibonding (p_z^-) states that either generate a nodal plane between the Sb atoms (antibonding p_z^-) or not (bonding p_z^+). These π-bonding states lie in an energy range above the occupied p^2 bonding states in the plane of the chain (p_x^- and p_y^-) and below the unoccupied p^2 antibonding states (p_x^+ and p_y^+). They are primarily responsible for the bonding of the Sb chain to the substrate because their charge distributions overlap with those of the dangling bond orbitals of the nearly unreconstructed substrate. These states lie in an energy range close to the valence-band edge (bonding to the substrate) and to the conduction-band edge (antibonding to the substrate). They are only half occupied for the isolated p^2-bonded Sb chain.

The alteration of the Sb-chain states when the chain is bonded to a GaAs(110) substrate is indicated in Fig. 4(a) and the orbital character of selected surface states at the $\bar{X}$ point are schematically depicted in Fig. 5. Comparison with Fig. 3 permits the identification of the origin of the top-layer Sb-derived surface-state bands for GaAs(110)-$p(1\times1)$-Sb(1 ML).

The occupied surface states S_1 and S_2 correspond to the nonbonding symmetric (s^+) and antisymmetric (s^-) s-like lone pairs within the Sb chain. These nonbonding states lie in an energy range within the heteropolar gap or close to it for most of the III-V substrates.

The occupied surface states S_3 and S_4 are associated predominately with the p^2-bonding states (p_x^- and p_y^-) in the plane of the Sb chain. They accumulate electronic charge density between the Sb atoms within the chain, and, as noted above, are responsible for the p^2 bonding in the plane of the chain. The energy of these states is such that they are located near the top of the stomach gap of

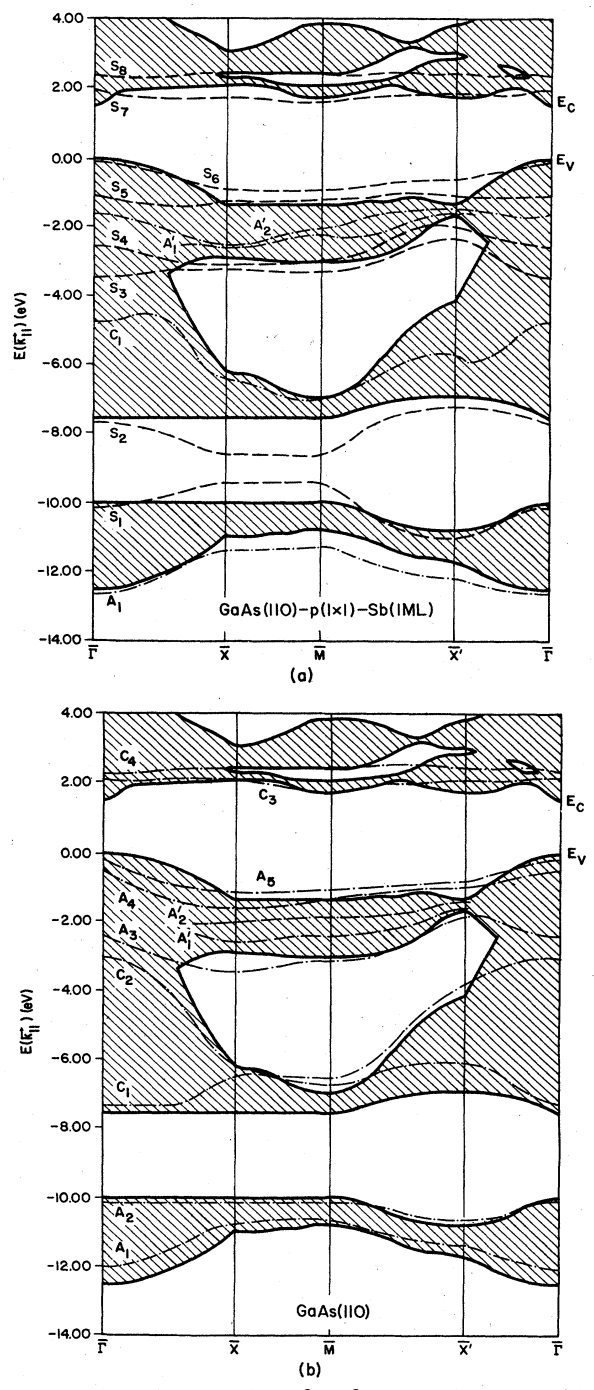

FIG. 4. Energy dispersion of surface bound states and resonances. (a) GaAs(110)-$p(1\times1)$-Sb(1 ML). Sb-derived surface states are denoted by S_n and indicated by a dashed line, whereas substrate-derived states are denoted by A_n and C_n and indicated by a dashed-dotted line. (b) Clean GaAs(110).

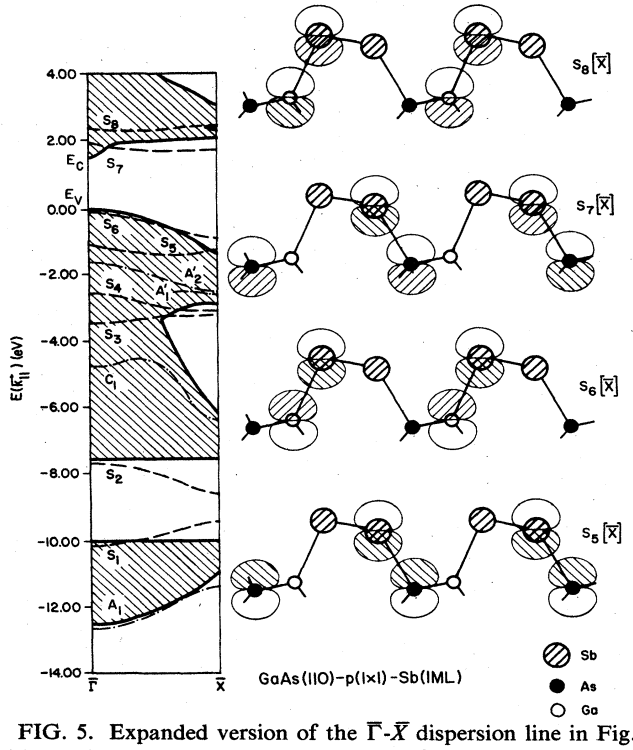

FIG. 5. Expanded version of the $\bar{\Gamma}$-$\bar{X}$ dispersion line in Fig. 4(a) together with a schematic indication of the orbitals associated with the surface states S_5, S_6, S_7, and S_8 at $\bar{X}$.

the projected band structure. The unoccupied antibonding combinations (p_x^+ and p_y^+) lie much higher in energy and are not shown. Some hybridization of the surface states S_3 and S_4 with the substrate orbitals occurs,[16] but the effect is rather small.

The occupied surface states S_5 and S_6 are associated with the π-bonding states (p_z^+) normal to the plane of the Sb chain. These states have a bonding character with high electronic density between the Sb chain and the substrate. The onoccupied π-antibonding partners (p_z^-) of these states are the surface states S_7 and S_8. These π-antibonding states have a low electronic density between the Sb chain and the substrate. Therefore, the bonding of the Sb chains to the substrate is generated by the mixing of the π states of the isolated chain with the dangling-bond orbitals of nearly unreconstructed substrate to form two occupied *bonding surface-state bands* [states S_5 and S_6] and two unoccupied *antibonding surface-state bands* [states S_7 and S_8]. The resulting Sb-substrate bonds are comprised of bonding combinations of sp^3 hybrid orbitals from the substrate and π-electron orbitals from the Sb chain. Thus, they are *not* conventional sp^3 bonds, although the minimum-energy structure is characterized by nearly sp^3 bond lengths and angles to the substrate. Such hybrid bonds are not characteristic of either bulk III-V compounds or their small molecule analogs. Hence they seem to exemplify a unique type of surface bonding characteristic of the $M_{\rm III}A_{\rm V}(110)$-$p(1\times1)$-Sb(1 ML) system. The occurrence of such surface bonds resolves the puzzle noted in the ELEED structure analysis[8] concerning simultaneous occurrence of the p^2 bonding within the Sb chain simultaneously with sp^3 bond angles of this chain relative to the GaAs(110) substrate.

From Fig. 5 we see that the topmost occupied surface state S_6 is associated with a *bonding* combination of the Sb-Ga charge densities, whereas the higher empty surface state S_8 corresponds to an *antibonding* combination of the Sb-Ga charge densities. Similarly, the lower occupied surface state S_5 is associated with a *bonding* combination of the Sb-As charge densities, whereas the bottommost empty surface state S_7 corresponds to an *antibonding* combination of the Sb-As charge densities. Simpler tight-binding models[1] have been utilized to predict that the energy eigenstate associated with the Sb—As bond lies lower in energy than the energy eigenstate associated with the Sb—Ga bond. This result is in agreement with ours, although the energies of the predicted eigenstates are somewhat different than the ones reported here.

As in the case of the single isolated p^2-bonded Sb chain, the surface-state energies show appreciable dispersion for $\mathbf{k}_{||}$ going from $\bar{\Gamma}$ to $\bar{X}$ along the chain direction, but no or little dispersion for $\mathbf{k}_{||}$ going from $\bar{X}$ to $\bar{M}$, perpendicular to the chain axis. In the case of an isolated Sb chain there is a symmetry-induced degeneracy of the surface states for $\mathbf{k}_{||}$ going from $\bar{X}$ to $\bar{M}$ due to the electronic equivalence of the two Sb atoms within the chain. If the two Sb atoms within the chain are electronically inequivalent, as occurs upon adsorption on a $M_{\rm III}A_{\rm V}(110)$ substrate, the resulting projected band structure exhibits an energy splitting of the surface states for $\mathbf{k}_{||}$ along the $\bar{X}$-$\bar{M}$ direction due to the polarity of the substrate. This result is evident in Fig. 4(a).

Our results for the surface-state eigenvalue spectrum for GaAs(110)-$p(1\times1)$-Sb(1 ML) are in good agreement with the self-consistent pseudopotential calculations of Bertoni *et al.*[16] which yield the surface-state eigenvalues at symmetry points of the (110) surface Brillouin zone. The geometry of the ordered Sb overlayer used by these authors is that determined by ELEED,[8] however, whereas we used the geometry determined by our sp^3s^* tight-binding total-energy minimization procedures. Since these geometries for the ordered Sb overlayers are essentially the same, (column 3 of Table IV), we expect the two calculations to agree well with each other, which they do. Our interpretation of the origins of the various Sb-derived surface-state bands differs, however, from that proposed in Ref. 16, in the cases of states S_3, S_4, S_5, and S_6. Since by using a tight-binding model we have direct access to the orbital character of the energy eigenvectors, we verified explicitly that S_3 and S_4 are predominately occupied intrachain Sb p^2-bonding orbitals, rather than the back-bonding hybrids proposed in Ref. 16. These orbitals do exhibit some back-bonding hybrid character, especially at the symmetry points $\bar{X}$ and $\bar{M}$, but the coefficients of these components of their wave function are small relative to those for the intrachain p bonding. The major occupied back-bonding surface states are S_5 and S_6, as illustrated in Fig. 5. The detailed nature of these orbitals is, of course, a function of $\mathbf{k}_{||}$. They reduce to the form shown in Fig. 5 of Bertoni *et al.*[16] at $\bar{X}'$ although the labels of S_5 and S_6 seem to be interchanged at that symmetry point in Ref. 16. The orbital character of each surface energy eigenstate at various symmetry points has also been identified by inspection of symmetry- and layer-resolved local density of state as calculated via the analytic Green's-function methodology (Sec. II E).

Having verified that our model predictions are compatible with the pseudopotential calculations for GaAs(110)-$p(1\times1)$-Sb(1 ML), we proceeded to evaluate the Sb-induced surface-state bands for the other Ga and In compounds. In panel (a) of Figs. 6—10 we display the energy dispersion of the surface states, projected onto the (110) surface Brillouin zone, of the overlayer systems $M_{\rm III}A_{\rm V}(110)$-$p(1\times1)$-Sb(1 ML) for GaP, GaSb, InP, InAs, and InSb, respectively, as the substrate. In each case the atomic structure used in the calculation of the surface-state eigenvalue spectrum is that defined by the set of structural parameters shown in Table IV. The results for all six surfaces are qualitatively similar, and display the same characteristics as those discussed above for GaAs.

The notation used to label the surface states of the overlayer systems $M_{\rm III}A_{\rm V}(110)$-$p(1\times1)$-Sb(1 ML) is that of Ref. 16, with S_n, A_n, and C_n denoting a surface state associated primarily with the overlayer Sb atoms, the substrate anion, or the substrate cation, respectively. For comparison purposes, we present the predicted surface-state dispersion relations for each of the clean (110) substrates in panel (b) of Figs. 4 and 6—10. We present a discussion of the distinguishing features between the electronic spectra of the Sb overlayers and those of the (110) surfaces of the clean substrates in the next section.

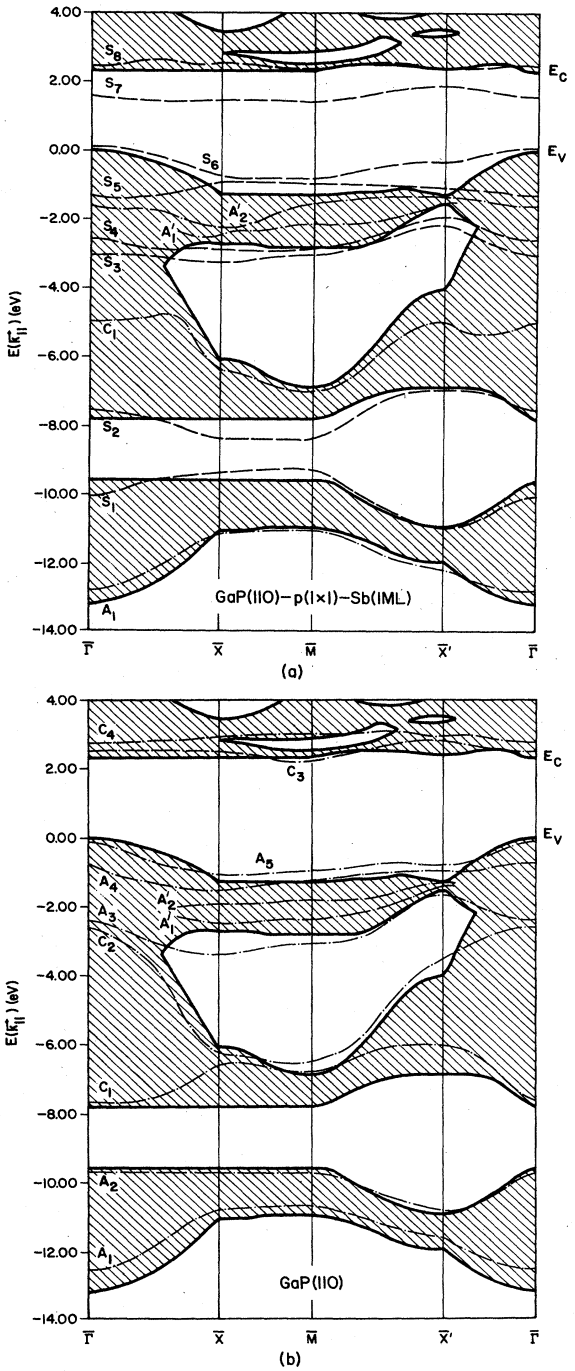

FIG. 6. Energy dispersion of surface bound states and resonances. (a) GaP(110)-$p(1\times1)$-Sb(1 ML). Sb-derived surface states are denoted by S_n and indicated by a dashed line, whereas substrate-derived states are denoted by A_n and C_n and indicated by a dashed-dotted line. (b) Clean GaP(110).

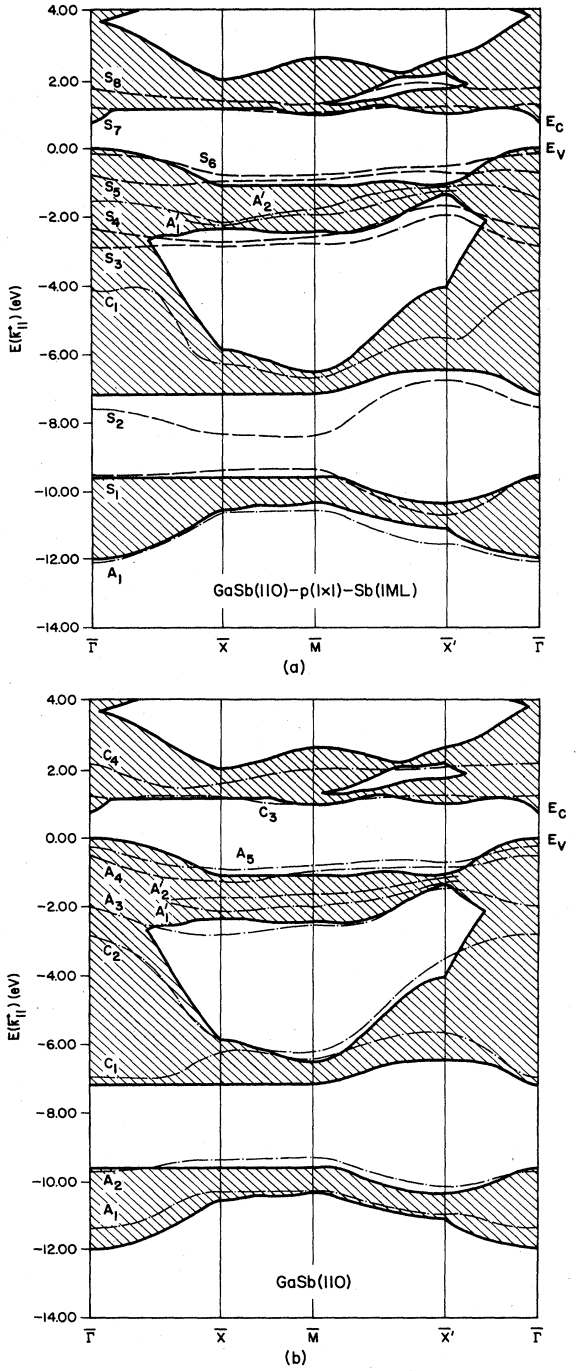

FIG. 7. Energy dispersion of surface bound states and resonances. (a) GaSb(110)-$p(1\times1)$-Sb(1 ML). Sb-derived surface states are denoted by S_n and indicated by a dashed line, whereas substrate-derived states are denoted by A_n and C_n and indicated by a dashed-dotted line. (b) Clean GaSb(110).

Another result of our systematic study of Sb overlayer systems is that, for all substrates except GaP(110), no *occupied* surface bound states are predicted to lie within the fundamental energy-band gap. For all overlayer systems studied, the maximum energy of the topmost occupied surface state S_6 is predicted to occur at $\bar{\Gamma}$ with a downward energy dispersion along the $\bar{\Gamma}\rightarrow\bar{X}$ and $\bar{\Gamma}\rightarrow\bar{X}'$ symmetry lines.

For most substrates, the topmost occupied surface state S_6 is predicted to be in resonance with the bulk bands with a maximum energy slightly below the valence-band maximum at $\bar{\Gamma}$. In the case of GaP(110)-

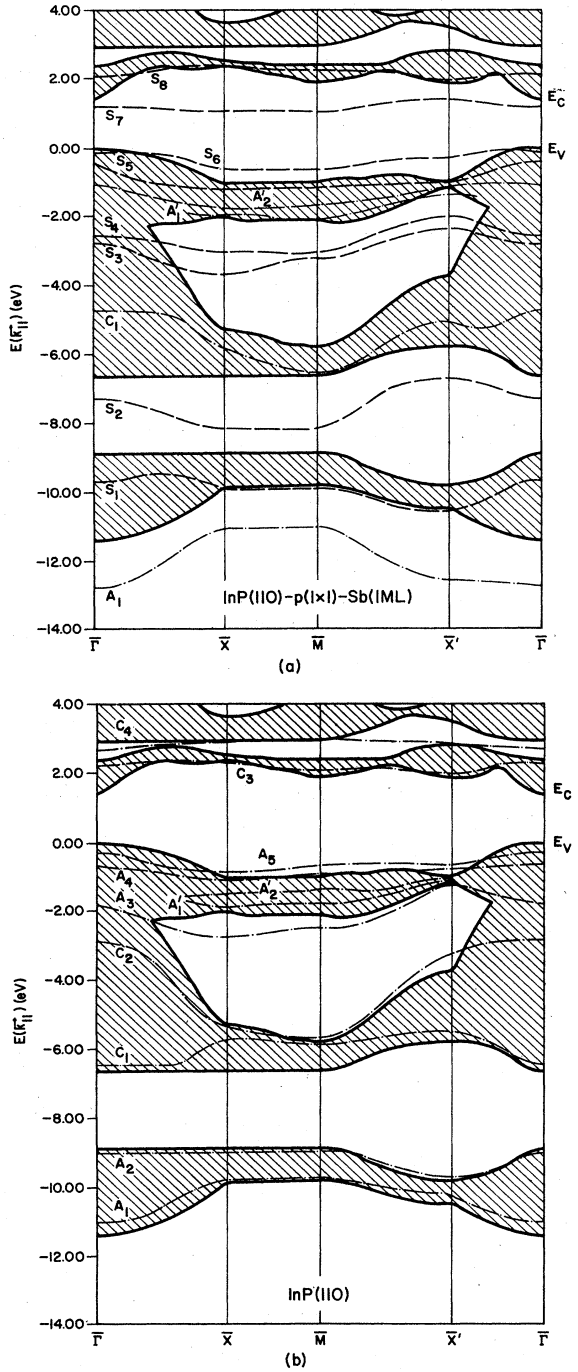

FIG. 8. Energy dispersion of surface bound states and resonances. (a) InP(110)-$p(1\times1)$-Sb(1 ML). Sb-derived surface states are denoted by S_n and indicated by a dashed line, whereas substrate-derived states are denoted by A_n and C_n and indicated by a dashed-dotted line. (b) Clean InP(110).

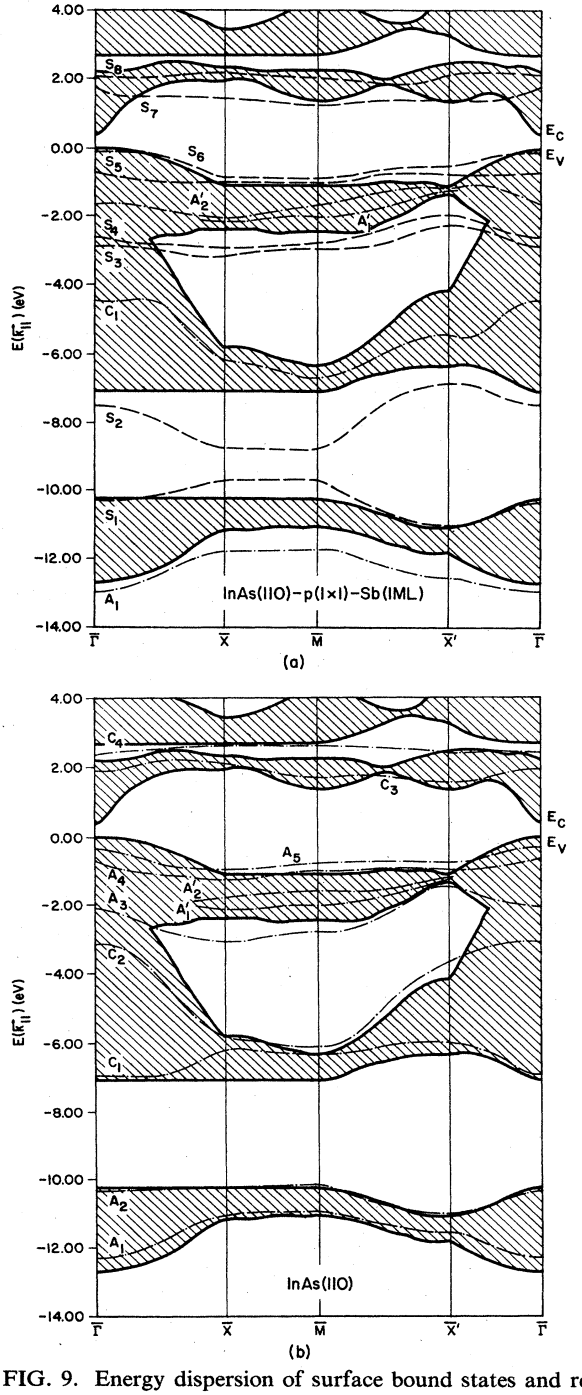

FIG. 9. Energy dispersion of surface bound states and resonances. (a) InAs(110)-$p(1\times1)$-Sb(1 ML). Sb-derived surface states are denoted by S_n and indicated by a dashed line, whereas substrate-derived states are denoted by A_n and C_n and indicated by a dashed-dotted line. (b) Clean InAs(110).

$p(1\times1)$-Sb(1 ML), the energy of the topmost occupied surface state S_6 is predicted to lie within the fundamental energy gap with a maximum energy of approximately 0.1 eV above the top of the valence band at $\bar{\Gamma}$.

C. Surface electronic states of Sb overlayers versus clean surfaces

Having determined the origin of the Sb-derived surface electronic states corresponding to ordered $p(1\times1)$ Sb

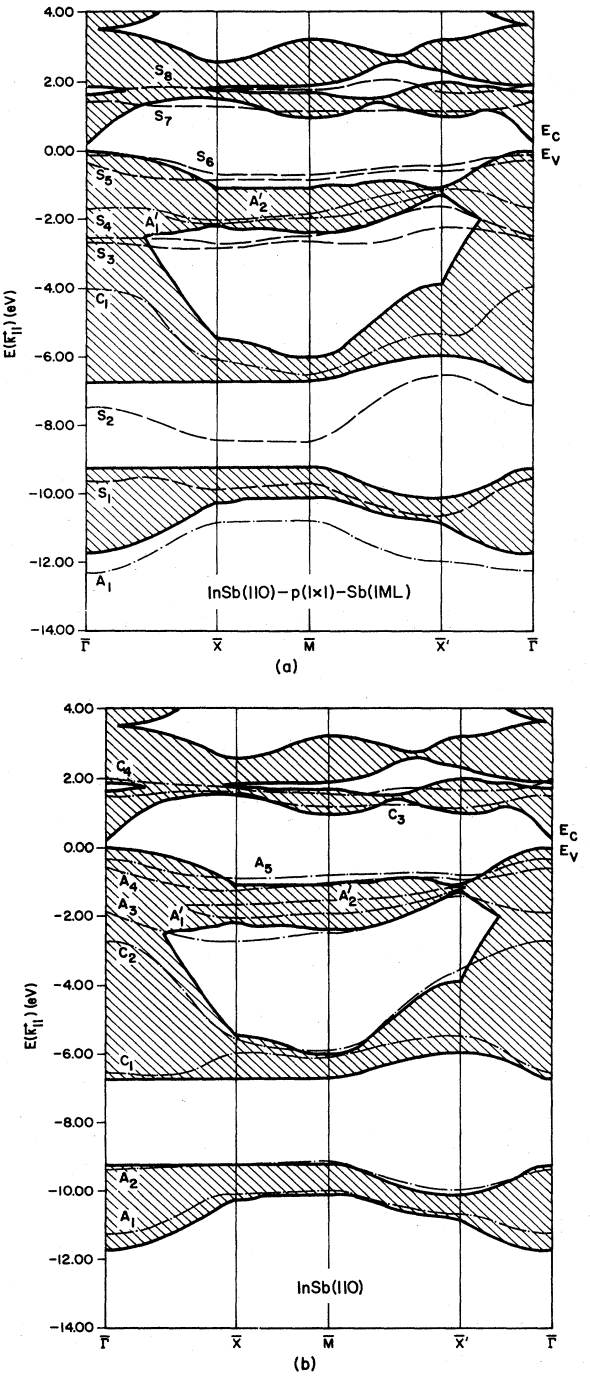

FIG. 10. Energy dispersion of surface bound states and resonances. (a) InSb(110)-$p(1\times1)$-Sb(1 ML). Sb-derived surface states are denoted by S_n and indicated by a dashed line, whereas substrate-derived states are denoted by A_n and C_n and indicated by a dashed-dotted line. (b) Clean InSb(110).

monolayers on the (110) surface of Ga and In compounds, we now compare their eigenvalue spectra with those associated with the corresponding relaxed clean (110) surfaces. The purpose of this comparison is to identify Sb-derived surface-state features and to suggest further ARPES experiments for Sb overlayer systems on Ga and In compounds. In order to identify the differences between the surface-state electronic spectrum corresponding to the ordered $p(1\times1)$ Sb overlayer and that associated with the clean (110) surface, we calculated the surface electronic state dispersion curves corresponding to each of the six substrates. The atomic relaxations of the clean (110) surfaces were determined by the total-energy minimization scheme employing the sp^3s^* tight-binding model described in Sec. II B. A detailed description of the resulting atomic geometries can be found in Ref. 37 along with a comparison with the structures experimentally determined via ELEED. Systematic dynamical calculations of elastic low-energy electron diffraction (ELEED) on the (110) surface of numerous III-V systems have established a common surface reconstruction pattern: the column-V element (anion) moves away from the bulk towards a pyramidal geometry, whereas the column-III element (cation) moves into the bulk towards a planar geometry.[2] The resulting surface structures are characterized by a large relative displacement perpendicular to the (110) surface of the cation and anion within the outermost layer $\Delta_{1,\perp}$ of the order of 0.6—0.9 Å.

The surface-state dispersion curves for the relaxed (110) surface of all six substrates are shown in panels (b) of Figs. 4 and 6—10. Direct comparison with the surface-state eigenvalue spectra of the corresponding Sb overlayer systems, displayed in panels (a) of these figures are readily made. The notation for the surface bound states and surface resonances for the clean (110) surfaces is that of Beres *et al.*,[30] with A_n (C_n) denoting states associated primarily with the anions (cations). Our predicted surface-state dispersion curves and orbital assignments are essentially identical to those of Beres *et al.*[30] for the clean (110) surfaces of both Ga-A_V and In-A_V compounds. This is hardly surprising because both our calculations and theirs employ the same sp^3s^* tight-binding model and the analytic Green's-function—effective Hamiltonian computational procedure, although the surface atomic geometry used by these authors for all (110) surfaces was a 27.3° bond-length-conserving rotation of the anion out of the surface plane and the cation into the bulk, rather than the minimum-energy geometries.

Before comparing the surface-state eigenvalue spectra of the ordered Sb overlayer system to those of the corresponding (110) clean substrate, it is useful to review the distinctive features associated with the surface electronic states of the relaxed (110) surface of III-V compounds. These features are qualitatively similar for all the clean (110) surfaces studied here as evident upon comparison of panels (b) of Figs. 4 and 6—10.

The occupied surface states A_2 and C_2 are mostly s-like in character and are localized in the first layer. The states A_1 and C_1 are also mainly s-like in character but are localized in the second layer. The surface states A_3, A_4, A_5, and C_3 are largely p-like in character. The highest occupied state A_5 is associated with the anion dangling bond and the lowest empty state C_3 is associated with the cation dangling bond. The occupied state A_4 is associated with the anion back-bonding band. Finally, the occupied surface resonances A'_1 and A'_2 and the surface band A_3 have mainly p-like character in the plane of the

(110) surface. They exhibit localization in both the first and second layers.

The orbital character of the surface electronic states found here is fully consistent with that reported by Beres *et al.*[30] Our surface-state eigenvalue spectra also are in agreement with self-consistent pseudopotential calculations in those cases where such calculations have been performed: i.e., GaAs(110),[42,43] GaP(110),[44] and InP(110).[45,46] Angle-resolved photoemission spectra have been obtained for GaAs(110) (Refs. 47–51) and InP(110) (Ref. 46). Our results are consistent with the qualitative features of these data, although the surface-state eigenvalue spectra extracted from the data are not identical in detail from one report to another.[48–51] Quantitative descriptions of selected results can be achieved for GaAs,[52] ZnSe,[52] and InP [i.e., compare Fig. 8(b) with Fig. 11 in Ref. 46].

Finally, we turn to the distinction between the electronic surface band spectra of the $p(1\times1)$ Sb overlayer systems and those of the clean (110) surfaces on which the overlayers are deposited. The individual distinguishing features can be identified by comparing panels (a) and (b), respectively, of Figs. 4 and 6–10.

The outstanding characteristic of $p(1\times1)$ Sb overlayers on (110) zinc-blende structure substrates is their generation of a surface-state eigenvalue spectrum analogous to that of a relaxed clean surface, but without requiring comparably large surface atomic relaxations. The origin of this result resides in the fact that Sb has five valence electrons, so large relaxations are not required to transfer charge from the surface cation to the surface anion in order to satisfy the local valence of each surface species. Since the geometries of the second and deeper layers are little changed between the clean surface and the adsorbed overlayers, the surface electronic states localized in the second layer in the case of the clean (110) surface are still present as substrate-derived states in the surface-state eigenvalue spectrum of the Sb overlayer systems, although their energies are shifted relative to their values for the relaxed clean surface. This observation describes the occupied *s*-like surface states A_1 and C_1 as well as the occupied *p*-like surface resonances A_1' and A_2' localized in the plane of the second layer. The occupied anion-derived surface states associated with dangling-bond bands (A_5) and back-bond bands (A_4) are replaced by the occupied surface states S_5 and S_6 associated with the hybrid bond consisting of the overlap of the π band of the Sb chain with the charge distribution of the substrate. In the particular case of GaAs(110)-$p(1\times1)$-Sb(1 ML), the lower occupied surface state S_5 corresponds to the Sb-As hybrid bond and the topmost occupied surface state S_6 corresponds to the Sb-Ga hybrid bond as can be seen from Fig. 5. Examination of the photoemission data by Skeath *et al.*[1] for GaAs(110)-$p(1\times1)$-Sb(1 ML) reveals that upon Sb deposition a surface feature at -2 eV disappears and another appears at -1.5 eV. We interpret this observation to result from the replacement of the As back-bond state A_4 by the surface state S_5 associated with the As-Sb hybrid bond. The *p*-like anion-derived surface state in the plane of the surface (A_3) has been replaced by the two predominantly intrachain (p_x^- and p_y^-) occupied bonding states S_3 and S_4. As mentioned above, these states are responsible for the bonding *within* the p^2-bonded Sb chain. Finally, the occupied *s*-like surface states A_2 and C_2 localized in the first layer have now been replaced by the bonding (S_1) and antibonding (S_2) combination of *s*-like Sb occupied lone pairs. As noted earlier, the energy of the occupied *s*-like lone-pair states lies within the heteropolar gap of all the compounds studied except for InP(110)-$p(1\times1)$-Sb(1 ML) and InSb(110)-$p(1\times1)$-Sb(1 ML).

Generally speaking, the differences between the electronic spectrum of the surface states associated with the Sb overlayers system and that of the corresponding clean (110) substrate appear to be universal for all the Ga and In compounds as evident from Figs. 4 and 6–10. GaP(110)-$p(1\times1)$-Sb(1 ML) is, however, a special case for which the *occupied* surface state S_6 is predicted to lie within the energy-band gap slightly above (0.1 eV) the top of the valence-band maximum. This is in contrast with the clean GaP(110) surface whose surface-state eigenvalue spectrum does not yield any *occupied* surface states within the energy-band gap. However, for both GaP(110)-$p(1\times1)$-Sb(1 ML) and the clean GaP(110) surface an *empty* surface state is predicted to lie within the energy-band gap. This finding for GaP(110) is in agreement with the calculations of Refs. 30 and 44 and the available experimental data.[53,54]

D. Atomic structure, surface bond lengths, and substrate ionicity

Given the common origin of the atomic geometries and surface states associated with Sb monolayers on the (110) surface of III-V semiconductor compounds, it is useful to correlate the surface atomic structure with the electronic nature of the substrate. Since the only available experimental measurements are ELEED intensity data for GaAs(110)-$p(1\times1)$-Sb(1 ML) and InP(110)-$p(1\times1)$-Sb(1 ML), and the structural parameter to which ELEED is most sensitive is the top-layer perpendicular shear between the two Sb atoms, $\Delta_{1,\perp}$, we relate $\Delta_{1,\perp}$ to the difference in character of the two substrate species.

The value of $\Delta_{1,\perp}$ is determined by two separate phenomena: the geometrical and electronic inequivalence of the anions and cations in the substrate. If the lengths of the Sb bonds to the substrate anions and cations are greatly different, then the p^2-bonded Sb chain will be tilted about the $\langle 110\rangle$ axis along the chain in the plane of the surface in order to minimize distortions of the bond lengths from their minimum-energy values. This phenomenon is primarily responsible for the large predicted values of $\Delta_{1,\perp}$ for InP and GaP substrates. Even if the Sb bonds to the anion and cation are approximately equal in length, however, the electronic inequivalence of the two substrate species will cause $\Delta_{1,\perp}$ to be nonzero. This phenomenon creates the small but finite values of $\Delta_{1,\perp}\simeq0.1$ Å for GaAs and InSb substrates. Indeed, for InSb $\Delta_{1,\perp}>0$, in spite of the fact that the Sb—Sb input bond length ($d=2.87$ Å) is taken to be slightly larger than the Sb—In bond length ($d=2.81$ Å).

Quantitative indications of these two trends are given in Fig. 11. In Fig. 11(a) the correlation between $\Delta_{1,\perp}$ and the

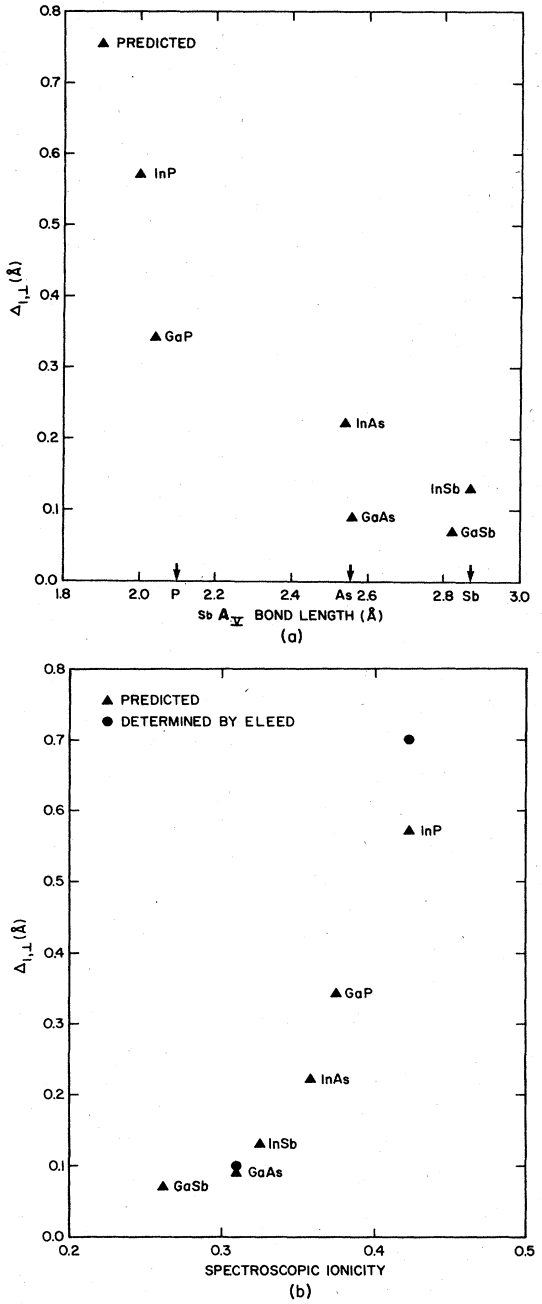

FIG. 11. (a) Predicted values of the relative displacement of the two Sb atoms perpendicular to the (110) surface, i.e., $\Delta_{1,\perp}$, plotted as a function of the minimum-energy Sb—A_V bond lengths for Ga and In compounds, respectively. The arrows indicate the value of the input bond length. The Ga—Sb input bond length is 2.65 Å and the In—Sb bond length is 2.81 Å. (b) $\Delta_{1,\perp}$ plotted against the spectroscopic ionicity (Ref. 49) of the substrate. The values obtained via ELEED are also shown for GaAs(110)-$p(1\times1)$-Sb(1 ML) (Ref. 8) and InP(110)-$p(1\times1)$-Sb(1 ML) (Ref. 41).

magnitude of the Sb—A_V bond lengths is shown. In Fig. 11(b) the predicted value of $\Delta_{1,\perp}$ is plotted against the Phillips[55] spectroscopic ionicity, f_i, for GaP, GaAs, GaSb, InP, InAs, and InSb. Although no simple correlation can be established between $\Delta_{1,\perp}$ and f_i, it is evident from this figure that $\Delta_{1,\perp}$ is a monotonically increasing function of the spectroscopic ionicity for a given column-III compound. The result emanates from the detailed energetics of the surface-state eigenvalue spectra of the unrelaxed (i.e., $\Delta_{1,\perp}\equiv0$) overlayer systems. An analysis of the surface-state eigenvalue spectra for the unrelaxed overlayer systems on the (110) surface of III-V compounds reveals that substrates with larger ionicity lead to higher energies for the occupied surface states S_5 and S_6 throughout the surface Brillouin zone. Upon atomic relaxation, these occupied states are reduced in energy, thereby lowering the total energy of the system. Substrates with larger ionicity therefore tend to produce larger shear between the two Sb atoms in order to minimize the total energy of the system. A similar phenomenon occurs for the atomic relaxation of the clean (110) surface of III-V and II-VI semiconductor compounds. In this case, however, the lowering in energy of the topmost occupied anion-derived dangling-bond surface state is accompanied by large shear ($\Delta_{1,\perp}\sim0.6$—0.9 Å) between the surface anion and cation. Attempts to correlate the magnitude of $\Delta_{1,\perp}$ with either the spectroscopic[55] or the Pauling[56] ionicities for clean (110) surfaces of III-V and II-VI compounds have failed,[57] however, and the magnitude of $\Delta_{1,\perp}$ is most closely related to measures of atomic size[58] as might be expected from the predominance of the bond-length effect [see, e.g., Fig. 11(a)] over the electronic inequivalence effect.

IV. SYNOPSIS

On the basis of a tight-binding model, we have predicted the atomic and electronic structure of ordered Sb monolayers on the (110) surfaces of GaP, GaAs, GaSb, InP, InAs, and InSb. The surface atomic geometries determined via total-energy minimization procedures are in agreement with those obtained from a published ELEED intensity analysis for GaAs(110)-$p(1\times1)$-Sb(1 ML) and a preliminary analysis for InP(110)-$p(1\times1)$-Sb(1 ML). Moreover, our predicted surface-state eigenvalue spectrum corresponds well to the eigenvalues obtained from self-consistent pseudopotential calculations performed at high-symmetry points in the surface Brillouin zone for GaAs(110)-$p(1\times1)$-Sb(1 ML). Our study indicates that there are three types of states occurring for a p^2-bonding Sb chain. The nonbonding (s-orbital-derived) states do not contribute to the Sb-substrate bonding. They are little affected by the substrate although the substrate polarity does split their degeneracy along the $\bar{X}$-$\bar{M}$ line. The intrachain bonding and antibonding p states also are not seriously affected by bonding to the substrate except for the $\bar{X}$-$\bar{M}$ splitting of their degeneracy for polar materials. These bonding p states are responsible for the Sb—Sb bonds within the individual p^2-bonded Sb chains. The bonding of the Sb chains to the substrate is generated by the mixing of the π states of the isolated chain with the dangling-bond orbitals of nearly unreconstructed substrate to form two occu-

pied bonding surface-state bands and two unoccupied antibonding surface-state bands. The resulting Sb-substrate bonds are comprised of bonding combinations of sp^3 hybrid orbitals from the substrate and π-electron orbitals from the Sb chain. They are not conventional sp^3 bonds, although the minimum-energy structure is characterized by nearly sp^3 bond lengths and angles to the substrate. Therefore our analysis reveals a novel type of hybrid Sb-substrate bonding which resolves a puzzle identified in the ELEED structure analysis of GaAs(110)-$p(1\times1)$-Sb(1 ML).

ACKNOWLEDGMENTS

The authors are indebted to A. Paton and A. Kahn for permission to use the preliminary results of the InP(110)-$p(1\times1)$-Sb(1 ML) structure, to D. Costenoble and L. J. Kennedy for assistance, and to M. D. Tabak for his generous support of this work. The authors gratefully acknowledge Professor Y. C. Chang of the University of Illinois whose complex-**k** band-structure computer program has been used in parts within the context of the calculation of the surface-state eigenvalue spectra.

[1]P. Skeath, C. Y. Su, W. A. Harrison, I. Lindau, and W. E. Spicer, Phys. Rev. B **27**, 6246 (1983).
[2]C. B. Duke, Adv. Ceram. **6**, 1 (1983); A. Kahn, Surf. Sci. Rep. **3**, 193 (1983).
[3]P. Skeath, I. Lindau, C. Y. Su, P. W. Chye, and W. E. Spicer, J. Vac. Sci. Technol. **17**, 511 (1980).
[4]P. Skeath, C. Y. Su, I. Lindau, and W. E. Spicer, J. Vac. Sci. Technol. **17**, 874 (1980).
[5]P. Skeath, I. Lindau, C. Y. Su, and W. E. Spicer, J. Vac. Sci. Technol. **19**, 556 (1981).
[6]P. Skeath, C. Y. Su, I. Lindau, and W. E. Spicer, Solid State Commun. **40**, 873 (1981).
[7]J. Carelli and A. Kahn, Surf. Sci. **116**, 380 (1982).
[8]C. B. Duke, A. Paton, W. K. Ford, A. Kahn, and J. Carelli, Phys. Rev. B **26**, 803 (1982).
[9]A. McKinley, G. J. Hughes, and R. H. Williams, J. Phys. C **15**, 7049 (1982).
[10]C. Stringer, A. McKinley, G. J. Hughes, and R. H. Williams, Vacuum **33**, 597 (1983).
[11]J. R. Chelikowsky, S. G. Louie, and M. L. Cohen, Solid State Commun. **20**, 641 (1976).
[12]D. J. Chadi and R. Z. Bachrach, J. Vac. Sci. Technol. **16**, 1159 (1979).
[13]E. J. Mele and J. D. Joannopoulos, Phys. Rev. Lett. **42**, 1094 (1979).
[14]A. Zunger, Phys. Rev. B **24**, 4372 (1981).
[15]J. Ihm and J. D. Joannopoulos, Phys. Rev. Lett. **47**, 679 (1981); J. Vac. Sci. Technol. **21**, 340 (1982).
[16]C. M. Bertoni, C. Calandra, F. Manghi, and E. Molinari, Phys. Rev. B **27**, 1251 (1983).
[17]C. Mailhiot, C. B. Duke, and Y. C. Chang, Phys. Rev. B **30**, 1109 (1984).
[18]P. Vogl, H. P. Hjalmarson, and J. D. Dow, J. Phys. Chem. Solids **44**, 365 (1983).
[19]D. J. Chadi, Phys. Rev. B **16**, 790 (1977).
[20]W. A. Harrison, *Electronic Structure and the Properties of Solids* (Freeman, San Francisco, 1980), pp. 443–452, 503–506.
[21]D. J. Chadi, Phys. Rev. Lett. **41**, 1062 (1978); Phys. Rev. B **19**, 2074 (1979); Vacuum **33**, 613 (1983).
[22]M. Schmeits, A. Mazur, and J. Pollmann, Phys. Rev. B **27**, 5012 (1983).
[23]H. Wendel and R. M. Martin, Phys. Rev. Lett. **40**, 950 (1978).
[24]K. C. Pandey and J. C. Phillips, Phys. Rev. Lett. **32**, 1433 (1974); **34**, 1450 (1975); Phys. Rev. B **13**, 750 (1976).
[25]R. E. Allen, Phys. Rev. B **19**, 917 (1979); **20**, 1454 (1979).
[26]J. Pollmann, in *Festkorperprobleme, Advances in Solid State Physics,* edited by J. Treusch (Vieweg, Braunschweig, 1980), Vol. XX, p. 117.
[27]Y. C. Chang and J. N. Schulman, Phys. Rev. B **25**, 3975 (1982).
[28]D. H. Lee and J. D. Joannopoulos, Phys. Rev. B **23**, 4988 (1981); **23**, 4997 (1981).
[29]J. Pollmann, A. Mazur, and M. Schmeits, Surf. Sci. **99**, 165 (1980).
[30]R. P. Beres, R. E. Allen, and J. D. Dow, Phys. Rev. B **26**, 769 (1982); **26**, 5702 (1982); Solid State Commun. **45**, 13 (1983).
[31]R. P. Beres, R. E. Allen, J. P. Buisson, M. A. Bowen, G. E. Blackwell, H. P. Hjalmarson, and J. D. Dow, J. Vac. Sci Technol. **21**, 548 (1982).
[32]H. P. Hjalmarson, P. Vogl, D. J. Wolford, and J. D. Dow, Phys. Rev. Lett. **44**, 810 (1980).
[33]H. P. Hjalmarson, H. Buttner, and J. D. Dow, Phys. Rev. B **24**, 6010 (1981).
[34]R. E. Allen and J. D. Dow, Phys. Rev. B **24**, 911 (1981).
[35]R. E. Allen, H. P. Hjalmarson, and J. D. Dow, Surf. Sci. **110**, L625 (1981).
[36]J. Ihm, D. H. Lee, J. D. Joannopoulos, and J. J. Xiong, Phys. Rev. Lett. **51**, 1872 (1983).
[37]C. Mailhiot, C. B. Duke, and D. J. Chadi, Surf. Sci. (to be published).
[38]S. T. Pantelides and J. Pollmann, J. Vac. Sci Technol. **16**, 1349 (1979).
[39]C. Kittel, *Introduction to Solid State Physics,* 3rd ed. (Wiley, New York, 1968), p. 105.
[40]D. J. Chadi, Phys. Rev. B **29**, 785 (1984).
[41]C. B. Duke, C. Mailhiot, A. Paton, and A. Kahn (unpublished).
[42]J. R. Chelikowski and M. L. Cohen, Phys. Rev. B **20**, 4150 (1979); Solid State Commun. **29**, 267 (1979).
[43]A. Zunger, Phys. Rev. B **22**, 959 (1980).
[44]F. Manghi, C. M. Bertoni, C. Calandra, and E. Molinari, Phys. Rev. B **24**, 6029 (1981).
[45]F. Manghi, E. Molinari, C. M. Bertoni, and C. Calandra, J. Phys. C **15**, 1099 (1982).
[46]G. P. Srivastava, I. Singh, V. Montgomery, and R. H. Williams, J. Phys. C **16**, 3627 (1983).
[47]N. V. Smith and M. M. Traum, Phys. Rev. Lett. **31**, 1247 (1973).
[48]J. A. Knapp and G. J. Lapeyre, J. Vac. Sci. Technol. **13**, 757 (1976).
[49]G. P. Williams, R. J. Smith, and G. J. Lapeyre, J. Vac. Sci. Technol. **15**, 1249 (1978).
[50]A. Huijser, J. van Laar, and T. L. van Rooy, Phys. Rev. Lett. **65A**, 337 (1978).
[51]J. A. Knapp, D. E. Eastman, K. C. Pandey, and F. Patella, J. Vac. Sci. Technol. **15**, 1252 (1978).
[52]C. Mailhiot, C. B. Duke, and Y. C. Chang, Phys. Rev. B **30**,

1109 (1984).
[53]A. Huijser and J. van Laar, Surf. Sci. **52**, 202 (1975); A. Huijser, J. van Laar, and T. L. van Rooy, *ibid.* **62**, 472 (1977).
[54]G. M. Guichar, C. A. Sebenne, and C. D. Thuault, J. Vac. Sci. Technol. **16**, 1212 (1979).
[55]J. C. Phillips, Rev. Mod. Phys. **42**, 317 (1970).
[56]L. Pauling, *The Nature of the Chemical Bond,* 3rd ed. (Cornell University, Ithaca, 1973), p. 93.
[57]C. B. Duke, A. Paton, and A. Kahn, J. Vac. Sci Technol. A **1**, 672 (1983).
[58]C. B. Duke, J. Vac. Sci. Technol B **1**, 732 (1983).